Metabolism fine tuning and cardiokines secretion represent adaptative responses of the heart to High Fat and High Sugar Diets in flies

Lucie Khamvongsa-Charbonnier, Laurent Kremmer, Magali Torres, Sallouha Krifa, Charis Aubert, Alice Corbet, Loic Crespo, Laurence Roder, Laurent Perrin, Nathalie Arquier

Metabolism fine tuning and cardiokines secretion represent adaptative responses of the heart to High Fat and High Sugar Diets in flies

Lucie Khamvongsa-Charbonnier[1,2,*], Laurent Kremmer[1,3,*], Magali Torres[1], Sallouha Krifa[1], Charis Aubert[1], Alice Corbet[1], Loïc Crespo[1], Laurence Röder[1], Laurent Perrin[1,4,#] and Nathalie Arquier[1,4,#,§]

1 Aix Marseille Univ, INSERM, TAGC, UMR_S_1090, 13288 Marseille, France
2 present address : CNRS UAR 3601, Institut Français de Bioinformatique (IFB), IFB-core,
3 present address : INRAE, Institut Sophia Agrobiotech, Université Côte d'Azur, CNRS, 06903 Sophia Antipolis, France
4 CNRS, 13288 Marseille, France

* equal contributions
# co-last authors
§ author for correspondence: nathalie.arquier@univ-amu.fr

Keywords: Cardiomyopathies, transcriptome, nutrition, cardiokines, *Drosophila*

SUMMARY

Cardiopathies are one of the leading causes of death in obese diabetics. Resulting in part from junk food, diabetic cardiomyopathies are notably characterized by contractile dysfunctions. Using the *Drosophila* model for cardiac function in pathophysiological context, we identified a set of candidate genes, expressed by the heart, whose expression is modulated by acute challenge on High Sugar and High Fat regimes. Genes encoding core components of key homeostatic pathways and proteins such as 1C-metabolism homeostasis, the Galactose metabolism pathway and metabolites transporters, were identified and characterized as adaptative factors of cardiac function under nutritional stresses. In addition, putative secreted proteins were found dysregulated, highlighting the heart as a secretory organ in hyperglycemia and hyperlipidemia. In particular, we characterized the Fit satiety hormone as a new fly cardiokine, which autonomously modulates the cardiac function and remotely affects feeding behavior. Overall, our study uncovered new roles for metabolic pathways and cardiokines, and highlights autonomous and systemic adjustable responses of the heart to nutritional stresses.

INTRODUCTION

Diabetes mellitus is a chronic metabolic disease characterized by hyperglycemia, affecting 9% of the world's adult population and responsible for 1.5 million deaths in 2019[1]. The pathophysiological causes and consequences of diabetes are numerous, which makes it a complex disease and a challenge for medicine. Heart diseases, one of the leading causes of death of type 2 diabetics, concern 35% of patients. Diabetic cardiomyopathies are characterized by contractile dysfunctions and structural changes without vascular disorders[2]. The etiology of these specific cardiac dysfunctions remains poorly understood due to the multiple causes of the disease onset. Excessive

circulating carbohydrates and lipids lead to insulin resistance in the cardiomyocytes, the trademark of type 2 diabetes (T2D), which concerns 90% of diabetic patients[1]. This induces a lack of glucose import and an abnormal fat accumulation in the cells[2]. Physiological consequences are mitochondria dysfunctions, lipotoxicity, oxidative stress and inflammatory pathways activations, as well as change in stiffness of the cardiac tissue by remodeling of the extracellular matrix (ECM), due to excessive glycation. Cellular dysfunctions can, in extreme cases, lead to cardiomyocyte apoptosis[2]. Resulting cardiac phenotypes are mostly diastolic dysfunctions and increased arrhythmias[2,3].

Drosophila, being the simplest model organism with a beating heart, is a valuable organism for the study of cardiogenesis, cardiac physiology and as well as cardiac performance and aging[4–7]. In recent years, it has become a model of choice for the study metabolic disorders and associated cardiomyopathies[8,9]. The adult cardiac tube is composed of around eighty cardiomyocytes which carry molecular, physiological, and mechanical properties similar to mammalian cardiomyocytes[10]. The contractile cells are in close proximity with a layer of forty pericardial cells, functionally and structurally similar to nephrocytes[11], with which they closely communicate to sustain their function[10,12]. The physiological equivalence between flies and mammals goes as far as metabolic perturbations' incidence on cardiac function. Indeed, pioneering studies have shown that flies fed High Fat or High Sugar Diets exhibit metabolic disorders and cardiac dysfunctions that are phenotypically reminiscent of mammalian diabetic-induced obesity and diabetic cardiomyopathies, such as abnormal lipidemia, cardiac dysrhythmias and tissue remodeling[9]. Highly conserved metabolic pathways were associated to cardiac perturbations resulting from excess of sugar[13] or fat[5,14,15] in the food (HSD_High Sugar Diet; HFD_High Fat Diet). It was shown that three weeks HSD feeding led to insulin resistance, body fat accumulation and cardiac fibrosis due to excessive collagen deposits[13]. Moreover, high circulating glucose levels induced activation of the hexosamine pathway in cardiac tissue which negatively impacted its contractile efficacy[13]. Like High Sugar, High Fat exposure for five days is sufficient to induce obesity and associated cardiac dysfunctions[14]. Indeed, in the fat body and in the heart, high lipids activated notably the TOR kinase pathway and its lipogenic targets (SREBP and FAS)[14]. More importantly, activated-TOR inhibited the expression of the ATGL/Brummer (Bmm) lipase as well as that of its target, the mitochondrial transcriptional co-activator PGC-1/Spargel (Srl)[15]. As a consequence, in addition to obesity, this cascade of molecular deregulations induced arrhythmias and excess fat content in the heart, leading to cardiac lipotoxicity, one of the most detrimental consequence of diabetic cardiomyopathies[9,15]. Recently, it was shown that the TORC2-complex subunit Rictor was induced by HFD, and that it reduced associated cardiac dysfunctions by promoting mitochondria fission in the heart[16].

In this study, we aimed at deciphering the genetic features underlying the cardiac dysfunctions upon nutritional stresses in order to better characterize the onset of diabetic cardiomyopathies.

Considering that the heart is itself directly affected by nutrition, we hypothesized that transcriptomic dysregulations would reflect how it can acutely adapt to this physiological stress. To this purpose, we analyzed the cardiac transcriptome of females fed HSD or HFD. Our analysis revealed dysregulation of core homeostatic components such as the one-carbon pathway, the galactose metabolism and metabolites transporters, that we characterized as key adaptative factors of the heart in response to nutritional stresses. We also observed that both HSD and HFD were accompanied by the dysregulation of a large number of genes encoding secreted proteins, which pointed out the involvement of cardiac myokines (cardiokines) in the adaptation to nutritional stresses. Notably, we identified the *fit* gene, encoding a satiety hormone[17], as a new fly cardiokine, expressed by cardiomyocytes and pericardial cells, that regulated cardiac function. Importantly, we also demonstrated that cardiac *fit* expression was able to remotely control food intake, further illustrating the adaptability of the heart to nutritional challenge.

RESULTS

High-Sugar and High-Fat Diets modified cardiac performance

In order to characterize the consequences of high nutrients supply on cardiac function, we first investigated how HSD and HFD affected the cardiac performance (Figure 1). Control females, expressing the cardiac Hand-Gal4 driver (written Hand> in this study), were challenged on normal diet (ND) and on two rich diets (HSD: ND supplemented with 30% sucrose; and HFD: ND supplemented 30% coconut oil, see Methods). Diets exposure lasted 10 days for HSD and of 3 days for HFD. We evaluated cardiac performance using the recently developed noninvasive high throughput assay, based on a heart specific fluorescent transgene, R94C02::tdTomato (attP2) (tdTk), that allows monitoring cardiac activity on intact, anaesthetized flies[18] (Figure 1A). Movies of 5s at 330fps were analyzed[19] to get precise quantification of heart structure and rhythm phenotypes (Figure 1A). Diameters of the cardiac tube at maximum contraction in systole (ESD, End Systolic Diameter) and when fully relaxed in diastole (EDD, End Diastolic Diameter), contractile efficiency (Fractional Shortening_FS = (EDD-ESD)/EDD ; equivalent to the ejection fraction), as well as duration of each heart beat (HP_Heart Period = SI + DI) comprising the contraction step (SI_Systolic Interval) and the relaxation step (DI_Diastolic Interval), were evaluated as previously shown[7]. Correlated phenotypes, such as the volume of circulating hemolymph in the heart per beat (Stroke Volume_SV) and the hemolymph flow rate (Cardiac Output_CO = SV/HP) were also estimated. HSD and HFD affected cardiac contractility as well as cardiac tube structure in control flies (Figure 1, S1). High Sugar decreased heart rate (significant increase of both HP and SI; heart rate= 1/HP), and tended to reduce Arrhythmia Index_(AI), (AI= std-dev(HP)/ mean HP) but had no significant effect on heart diameters or contraction efficiency (ESD, EDD, FS) (Figure 1B-H). High Fat tended to induce cardiac

hypertrophy, as suggested by enlarged systolic and diastolic diameters (ESD, EDD, Figure 1F-G) and this was associated to increased Fractional Shortening (FS), Stroke Volume (SV) and Cardiac Output (CO), which may suggest a compensatory increase of contraction efficiency (Figure 1H-J). However, HP, DI, SI and AI were not affected, indicating that 3 days of HFD did not lead to heart rate and rhythm defects (Figure 1B-E). Previous studies, using *ex vivo* preparations of adult hearts[20], showed that adult flies fed HSD and HFD for 3 weeks displayed increased Arrhythmias and reduced Fractional Shortening[9]. This discrepancy could be due to the duration of the nutritional challenge but also to the non-invasive method used here to evaluate the phenotypes.

Analysis of the fly cardiac transcriptome upon nutritional stress

To decipher the molecular perturbations induced by HSD or HFD, we analyzed the cardiac transcriptome of females fed each of these diets. Three replicates of 30 hearts were dissected for each diet and sequenced on Illumina NextSeq 500 (Figure 2A). Reads were aligned on dm3 genome annotation and reannotated with dm6 release. After trimming and normalization, 9981 genes were found expressed in cardiac tissue and were subjected to differential expression analysis using both DEseq2_RLE[21] and edgeR_TMM[22] (HSD: Figure S2A-C; HFD: Figure S2D-F). Genes found differentially expressed (fold change > 1,5, adjusted p val < 0,05) with both methods were retained. Compared to ND, respectively 452 (354 down-regulated/80 up-regulated) and 254 (174 down-regulated/80 up-regulated) differentially expressed genes (DEG) were identified in HSD and HFD (Figure 2B-D and Table S1). Detailed analysis of the 110 common DEG between HSD/HFD *vs* ND, showed that 75 had the same pattern (Figure 2E) and 35 the opposite when compared to ND (Figure 2F). Enrichment analyses using PANGEA[23,24], focused on KEGG annotations, were performed separately on DEG identified in HSD and in HFD *vs* ND. HSD highlighted carbohydrates and amino-acid metabolism pathways (Figure 2G-H), whereas HFD highlighted lipid, amino-acid and hormone synthesis pathways (Figure 2I-J). 443 genes were differentially expressed in HSD compared to HFD, but we did not analyze them independently (HSD *vs* HFD, Figure 2D; sugar_*vs*_fat, Table S1). Overall, our data displayed the modulation of fundamental metabolic processes in the heart upon HSD and HFD (Figure H,J), suggesting a fine tuning of cardiac physiology in nutritional stresses. We therefore tested whether identified deregulated genes allow adaptative responses of the cardiac function upon these nutritional stresses.

High Sugar Diet downregulated 1C-metabolism and Leloir galactose pathways

Several genes encoding enzymes associated to 1C-metabolism pathway were found overrepresented in HSD versus ND (Figure 2G-H; Figure S2G). 1C-metabolism pathway is a fundamental homeostasis network, which includes several connected pathways involved in methylation (methionine cycle),

trans-sulfuration and nucleotide synthesis (folate cycle)[25]. Methionine cycle results in the production of S-adenosylmethionine (SAM), the universal donor of methyl-group in the cell[26]. Among the methyl-transferases that regulates the pool of cellular SAM, GNMT (Glycine-N-methyl transferase) has been involved in the catabolic process of SAM to SAH (S-adenosylhomocysteine), by conversion of Glycine into Sarcosine (N-methylated derivate of Glycine) in the liver in humans[26] (Figure 3A). SARDH (Sarcosine dehydrogenase) proceeds to the reversal conversion (Figure 3A). Expressed in Drosophila cardiac cells (Fly Cell Atlas[27]), *Gnmt* was downregulated in both diets (log2FC: -3.4 in HSD and -5.29 in HFD) while *Sardh* in HSD only (log2FC: -2.05). To evaluate the role of 1C-metabolism in the heart, knockdown of both *Gnmt* and *Sardh* were performed with the cardiac specific driver Hand-Gal4. Cardiac performance phenotypes were analyzed using the live-imaging set-up described above (Figure 3B-F). In ND, hypertrophy of the cardiac tube was observed following both KD (increase of both ESD and EDD) (Figure 3C; S3B). This was associated to an augmented CO (Cardiac Output) (Figure S3A). In HSD, *Gnmt* KD led to reduced Heart Period (HP) and Arrythmia Index (AI) (Figure 3D-E), suggesting that it is able to counteract the effect of HSD observed in control flies on these phenotypes (Figure 1B,E). *Gnmt* KD in HSD also resulted in increased ESD, FS and CO (Figure 3C,F; S3A), suggesting improved contractile efficacy in HSD compared to ND (Figure 3F vs Figure S3C-E). This showed that *Gnmt* inhibition induced cardiac hypertrophy but also that it reversed rhythm alterations induced by sugar, suggesting a protective effect.

HSD also dysregulated enzymes from the Leloir pathway, which are converting D-Galactose into Glucose-1P (Figure 3G). *CG32444/Galm1* (*GalM* orthologue) and *Galk* are both slightly downregulated in HSD (log2FC: -1.3 and -1.01 respectively) and strongly expressed in cardiac cells[27]. Fly orthologues of *GalT* and *GalE* were also downregulated, but however did not reached significance (Table S2). In ND, *Galk* KD was associated to decreased HP and DI (Figure 3H-J), showing that the effect of *Galk* accelerated heart rate by reducing relaxation time. In HSD, *Galk* KD did not result in HP and DI changes (Figure 3H-J) compared to control flies, showing that *Galk* function in rhythm modulation is not dominant over diet effect in this context. Previous reports have identified *Galk* gene as a suppressor of Calcineurin-induced cardiac dilatation in flies, with no cardiac phenotype by itself when mutated[28]. Our analysis however showed that in normal nutritional context, decreasing *Galk* expression in cardiac cells is sufficient to significantly modulate cardiac rhythm.

High Fat Diet modulated CD36-scavenger receptor and GLUT8 orthologues

One of the most significant DEG identified in HFD is the *Snmp1* gene (Figure 2C), which was found downregulated in this stress (log2FC: -2). *Snmp1* encodes the orthologue of the CD36-scavenger receptor and is strongly expressed in cardiac cells (FlyCellAtlas[27]). *Snmp1* was previously shown to promote FA transport in cells of the larval prothoracic glands and in ovaries, downstream of

SUMOylation processes[29], demonstrating its role in FA metabolism. In human cardiomyocytes, fatty acids (FA) and glucose imports both contribute to reach the ATP needs of cardiac contractile cells. FA are the main energetic source of cardiomyocytes, being metabolized by mitochondrial oxidation. Insulin induces both the FA transporter CD36-scavenger receptor (CD36-SR-B3) and GLUT4 hexose transporter translocation to the membrane[30]. In insulin-resistance context, GLUT4 mis-translocation and CD36 stabilization result in glucose deficit and FA accumulation[2].We observed that in heart of females fed ND, both *Snmp1* KD and overexpression (OE) displayed marked structural phenotypes (Figure 3K-M). EDD and ESD were both reduced upon KD and OE (Figure 3L; S3F). Modified heart diameters additionally impacted FS in *Snmp1* KD (Figure 3M). Abnormal and defective ostia were observed in 100% of *Snmp1*^{WT} OE hearts (Figure 3K, white stars) and were associated to arrhythmias amplification (Figure S3G). We also noticed that *Snmp1* KD adults were fattier than controls. Indeed, distinct fat tissue in the abdomen and surrounding the heart was observed in 66% of the imaged KD-females vs 25% in the controls (Figure S3I). Strong lethality resulting from 3 days HFD exposure in *Snmp1* KD, made it impossible to analyze. Nevertheless, our results highlighted a new role of *Snmp1* in autonomous cardiac function with a systemic side-effect on body lipid homeostasis.

As a parallel, HFD slightly induced the expression of *nebulosa (nebu)* gene (log2FC: 0.6), which encodes an orthologue of the human SLC2A8/GLUT8 hexose transporter. Recently, GLUT8 was identified as an insulin-dependent cardiac hexose transporter in mice, whose expression is strongly reduced in diabetes[31], but its function is not characterized. Fly gene *nebu* is highly expressed in cardiac cells (FlyCellAtlas[27]). In ND (Figure 3N-P), inhibition of *nebu* expression triggered heart constriction (reduction of heart diameters both in systole and diastole; Figure 3O-P) and increased heart rate (revealed by a reduction of HP and DI; Figure S3J-K). This showed that the cardiac tube is reduced in size and displayed accelerated beats compared to control. A reduced cardiac flux of hemolymph (Stroke Volume, Figure S3L) was also observed as a consequence. In HFD, *nebu* KD, did not affect the heart diameters (Figure 3O-P), but still significantly reduced HP (Figure S3J). This suggested that the effect of *nebu* on heart contractility is not dependent on diet. Previously identified as a regulator of sugar tolerance[32], *nebu* is shown here as a regulator of cardiac function.

HSD and HFD revealed the secretory function of the heart

gProfiler[33] (https://biit.cs.ut.ee/gprofiler/gost) analysis pointed to an enrichment of genes annotated as localized in the extracellular space (GO terms: extracellular region/space) among DEG in both HSD and HFD compared to ND (Figure S4A). Using the BioMart[34] (https://www.ensembl.org/info/data/biomart/index.html) and SignalP[35] (https://services.healthtech.dtu.dk/services/SignalP-5.0/) prediction tools, we identified 123 (in HSD) and 114 (in HFD) cardiac genes encoding putative secreted proteins that are mis-expressed (Figure

S4B, Table S3). 51 genes are dysregulated in both diets, including 26 with a characterized human orthologue (Table S4). 22 of these orthologues have been identified in Genome Wide Association Studies (GWAS), exhibiting common variants associated with metabolic or cardiac phenotypes (source "human genetics common metabolic disease knowledge portal", CMD-KP; https://md.hugeamp.org/) (Table S4). Based on homology score (DIOPT[24]) and on the phenotypes associated to their human orthologues, we selected 12 fly genes for specific knockdown in the heart (Figure 4A). *ImpL2*, *Yp1, Yp2, Yp3*, *CG3513*, *Nepl10*, *CG7997*, *phu*, *GILT2*, *CG34357* knock down revealed phenotypes reminiscent of the cardiac function related to–their orthologues (Figure 4A). Except *phu* and *Invadolysin* (which are inversely dysregulated in HSD and HFD) (Table S1) and *ImpL2* (which is upregulated in both diets), *Yp1-3, CG3513*, *Nepl10*, *CG7997*, *GILT2* and *CG34357* are all downregulated following nutritional stresses. Cardiac expression knockdown of *Yp2*, *CG3513*, *Nepl10*, *CG7997*, *phu*, *GILT2* and *CG34357* in ND were associated with modifications of heart diameters and rate (Figure 4A, fifth column). We observed decreased HP when knocking down *CG32357*, *GILT2*, *CG3513*, *Yp2*, *CG7997* and *Nepl10* (Figure 4B), which resulted from reduction of SI (Figure 4D) and/or DI (Figure S4C). In contrast, both *phu* and *ImpL2* exhibited increased HP (Figure 4B) resulting from extension of the contraction period (SI; Figure 4D). Contractile dysfunction, characterized by a reduced FS, was associated to *Yp2* and *CG7997* knockdown (Figure 4C), consecutive to enlarged ESD (Figure S4D). *phu* KD also resulted in cardiac hypertrophy (Figure 4E). Despite a high expression in the heart (FlyCellAtlas[27]), knocking down *Invadolysin* led to no detectable cardiac dysfunction (Figure S4F-G as example). Overall, our results strongly suggest that the identified DEG encoding secreted proteins we tested would be putative cardiokines and their human orthologues may be involved in metabolic disorders-associated cardiomyopathies.

Cardiac Fit expression impacted cardiac performance

The gene encoding Fit, a satiety hormone[17], was identified as downregulated both in HSD (log2FC: -1.55) and HFD (log2FC: -2.26). In ND, by knocking down its expression (*fit* KD written *fitKK*) in the whole heart (WH) with Hand> (Figure 5A; S5A) as well as in the cardiomyocytes (CM; tinCD4-Gal4, written tinCD4>; Figure S5A) or pericardial cells (PC; Dot-Gal4 written Dot>; Figure S5A) independently (Figure 5B-C), we observed a reduction of heart period, indicating that cardiac *fit* expression impinged on heart rhythm. Hand> knockdown induced the strongest phenotypes, resulting from both SI and DI reductions (Figure S5B-C), but consistent phenotypes observed using Dot> and tinCD4> revealed that *fit* expression from both PC and CC contributed to *fit* function in the heart. A decrease in AI was additionally noticed with all 3 drivers, confirming our previous observation (Figure 5D). Conversely, overexpressing (OE) *fit* (fit^{WT}) using Hand> is enough to

significantly increase HP, with a similar trend with Dot>, although this latter driver did not reached significance (Figure 5A-C). Likewise, overexpression of *fit* from a non-cardiac tissue (in the fat body with Lsp2-Gal4, noted Lsp2>) led to HP increase (Figure 5E), suggesting that fat-secreted Fit is also able to remotely control cardiac rhythm. Taken together, *fit* KD and OE experiments indicated that *fit* expression in cardiac tissue is involved in heart rhythm control and that Fit protein expressed from heart tissue acted *via* an autocrine and/or paracrine *modus operandi*. In HSD, which led to an increased HP in control flies (Figure 1B), knocking down *fit* with *fitKK* or *fitGD* strongly shortened HP, mainly by reducing SI (Figure 5F, S5B-F). *fitGD* but not *fitKK* additionally reduced AI in this nutritional context (Figure S5G-H). Moreover, the cardiac hypertrophy observed in control flies in HFD (Figure 1F-G) tended to be reduced upon *fit* KD (Figure 5G). This indicated that *fit* downregulation might contribute to a reduction of HSD-induced arrhythmias and HFD-induced hypertrophy. Taken together, these results showed that cardiac Fit modulated heart rhythm in ND and counteracted the deleterious effect of nutritional stresses when strongly downregulated (see Figure 6F).

Fit, a cardiokine regulating feeding behavior

Fit has been previously identified as a satiety hormone secreted by the fat body, which regulates food intake by promoting insulin secretion from the IPCs[17]. To evaluate the role of cardiac *fit* in feeding behavior, 1week-old females were starved overnight and then fed ND supplemented with Erioglaucine blue dye for 3hours. Blue food content in gut – a readout for food intake monitoring - was measured by OD at 629nm on lysates obtained by crashing decapitated flies (see Methods). As shown in Figure 6A, we detected an increase of feeding when knocking down *fit* expression in the heart. The same trend- although not significant- was observed following KD restricted to CC or to PC (Figure 6A). Conversely, overexpressing *fit* tended to reduce feeding behavior, this phenotype being exacerbated following OE restricted to PC (Figure 6B). These results indicated that Fit secreted from heart cells had a remote effect on a complex behavior such as food intake. We then tested if cardiac Fit could be secreted into the hemolymph. As shown in Figure 6C, we could indeed detect tagged Fit (Fit-HA) in hemolymph extracts when expressed in cardiac cells with Hand>. In order to decipher if feeding modulation by cardiac *fit* may be mediated by insulin release from the insulin producing cells (IPCs), we performed Dilp5 immunostaining in adult brains. Dilp5 is one of the functional orthologues of human insulin in *Drosophila*[36], produced and secreted by the IPCs (for Insulin Producing Cells) which are neuroendocrine cells of the *pars intercerebralis* region of the brain. Diet-dependent Dilp5 content in the IPCs, detected by immunostaining, reflects its active secretion (low or no staining) or its accumulation (strong staining)[37]. As already described[37], we quantified a strong Dilp5 accumulation in the IPCs following overnight starvation, in brains of control flies and of cardiac *fit* knockdown or overexpression (Figure 6D, left panels; Figure 6E). Following 3 hours of refeeding,

cardiac *fit* knockdown was insufficient to significantly affect Dilp5 accumulation (Figure 6D,E) but *fit* overexpressing flies in the heart displayed reduced Dilp5 levels in the IPCs compared to refed controls (Figure 6D, right panels, Figure 6E). Similar trend was observed following modulation of *fit* expression in the pericardial cells with Dot> (Figure S6A). These observations showed that Fit secreted from the heart was sufficient to remotely modulate Drosophila insulin content in the IPCs, which eventually resulted in the modulation of feeding behavior. All together, these results indicated that the adult heart remotely impeded on systemic metabolic homeostasis and that cardiac *fit* played a key role in this process.

DISCUSSION

Metabolic homeostasis has to be tightly regulated to avoid irreversible dysregulations that would lead to severe pathologic situations. Resulting notably from an unhealthy diet, obese diabetics often suffer from cardiomyopathies. In this study, we used *Drosophila* to decipher the genetic and molecular impacts of acute High Sugar/High Fat food challenge on cardiac function. Our results revealed key metabolic pathways dysregulated in the heart in order to autonomously adapt the cardiac function to nutritional stresses. 1C-metabolism and Galactose metabolism in HSD, as well as metabolites import transporters in HFD were highlighted. Additionally, we identified numerous putative secreted proteins, suggesting that heart is able to non-autonomously adapt to diets. Strikingly, we uncovered the cardiac function of the satiety hormone Fit, that impinged locally on cardiac performance (via both autocrine and paracrine actions) and remotely on feeding behavior, characterizing it as a new cardiokine.

Members of both 1C-metabolism and Leloir pathways were downregulated in HSD. The Glycine-N-methyl transferase (GNMT) is a key enzyme of the methyl-group donor pool homeostasis. It directly regulates the amount of S-adenosylmethionine (SAM), and its derivative SAH, by conversion of Glycine into Sarcosine. Downregulation of *Gnmt* led to cardiac dilatation and did not affect heart rhythm in ND, whereas in HSD, *Gnmt* KD rescued the sugar-induced HP increase. Contractile efficacy was improved in HSD *Gnmt* KD females and arrhythmias was decreased, suggesting a protective role. In fly fat body, *Gnmt* KD was shown to trigger SAM accumulation and Sarcosine depletion[38]. While no report to date established a causal link between cardiac SAM levels and heart diseases in mammals, high circulating SAH level was shown to be of bad prognosis for CVD[39]. Then, would high SAM level in the heart be beneficial is not known. The circulating level of Glycine, substrate of GNMT for methyl-group transfer (Figure 3A) was shown to be inversely correlated to CVD risk[40]. High Glycine and high SAM, both resulting from GNMT activity inhibition, could be responsible for the preserved contractile function in HSD fed flies.

Sugar stress also downregulated the expression of *Galactokinase* (*Galk*) gene. Galk is involved in the production of Galactose-1P[41] (Figure 3G). We showed that, in the heart, *Galk* KD slowed down heart beats in ND but had no consequences on heart function in HSD. The lack of Gal-1P production could compromise the subsequent Glucose-1P production. As a consequence, ATP production in cardiomyocytes could be impacted, explaining contractile dysfunctions. Previously shown as a suppressor of Calcineurin function in fly heart[28], our analysis characterized its autonomous cardiac function. Several members of the Galactose catabolism were identified in our analysis, reinforcing a yet uncharacterized cardiac role of the Leloir pathway in the heart.

We also reveal that HFD feeding upregulated the insulin-dependent fatty acids and glucose transporters orthologues, CD36-scavenger (Snmp1) and GLUT8 (Nebulosa, Nebu). Inhibition and overexpression of *Snmp1* induced acute morphological and contractile defects. Given its known function as a regulator of fat metabolism[29], we hypothesize that increasing FA import by *Snmp1* OE in the heart may lead to FA-oxidation excess, overloading mitochondria function and finally inducing lipotoxicity. We noticed that *Snmp1* KD adults were clearly fattier than controls. Decreasing FA import by cardiac-*Snmp1* KD could result in an enhancement of organismal adiposity, and consequently to cardiac lipotoxicity, as it has been previously shown[15]. These results support a systemic role for cardiac Snmp1 on lipid homeostasis.

The *nebu* KD females displayed reduced cardiac tube diameters in ND and accelerated heart rhythm in both diets. As its mammalian orthologue *GLUT8*, *nebulosa* gene is strongly expressed in the heart. GLUT8 function in the heart is not well characterized in mammals, but was shown to be associated to high atrial fibrillation in insulin-resistant mice[42]. Here, we show that GLUT8 fly orthologue KD is sufficient to compensate for the diastolic phenotype induced by HFD.

Collectively, our results suggest that the dysregulated genes identified are important for the integrity of cardiac function under HSD and/or HFD. This highlights the heart as a metabolic tissue, whose dysfunctions are partly dependent on an autonomous response to nutritional stresses. Our analysis also showed that the heart exhibits a non-autonomous response to nutritional stresses. Indeed, 27% (123/452) in HSD and 45% (114/254) in HFD of the DEG identified encoded putative or known secreted proteins. Cardiac genetic invalidation was preferentially performed on those having a human orthologue with potential metabolic and/or cardiac function. Eight over nine tested genes were shown to participate in cardiac performance regulation. This strongly suggests that our analysis is relevant for the identification of secreted cardiac factors. Further studies aimed at deciphering their systemic role will be necessary to classify them as cardiokines. Indeed, one of our cardiokine candidate, *ImpL2,* has previously been identified as an IGF-binding protein[43,44]. It was shown as a cachexia-promoting factor, being secreted from midgut tumoral cells[45,46]. In the cardiac cells,

stressed by HSD or HFD, secreted ImpL2 could also, as a cardiokine, affect peripheral tissues physiology.

Finally, we focused on the *fit* (*female-independent of transformer*) gene. Characterized as a fat-secreted satiety hormone in response to protein feeding[17], and regulating sugar intake for sustained egg laying in females[47], its expression is downregulated in response to both HSD and HFD in the heart. In ND, we demonstrated that inhibiting its expression in the heart increased heart rate and further established that Fit is required in both cardiomyocytes and in pericardial cells. Indeed, targeting *fit* KD in these two populations independently recapitulated the rhythm defects. Overexpression of *fit* in the heart or fat body reduced the heart rate, showing that Fit exerts its function in an autocrine/paracrine manner. In agreement with this observation, we showed that Fit is secreted into the hemolymph when expressed from the heart. In addition, lowering cardiac *fit* expression has a protective effect on cardiac function under nutritional stresses, since it was sufficient to counteract the HSD-induced low heart rate and HFD- induced cardiac hypertrophy. We also demonstrated that cardiac *fit* remotely impinged on food intake. This was correlated to Insulin level in the IPCs, suggesting that secreted cardiac Fit could signal to the adult brain to regulate feeding behavior. Expressed by cardiac cells to autonomously control cardiac function and systemically modulate feeding, Fit is clearly a fly cardiokine. Studies in mammals identified some cardiokines which act in an autocrine/paracrine manner[48]. These proteins have been mainly characterized in response to cardiomyocyte stresses, remodeling processes, but also in remote control of metabolic homeostasis[49,50]. Natriuretic peptides (ANP and BNP), several cytokines, growth factors (FGFs, VEGF) and neuropeptides (like MANF), constitute known cardiokines expressed by cardiac- and cardiac-associated cells (ECM cells, fibroblasts, epicardial adipose tissue)[48]. They have been detected in the blood and shown to act as paracrine and systemic signals upon cardiac injury[48,49]. In flies, different studies identified proteins secreted from cardiac cells as regulators of lipid homeostasis and organismal obesity[51–53]. However, we identify for the first time, a protein secreted by the heart, which not only changes cardiac performance but also affects a complex behavior, such as food intake. Finally, our results highlight the heart as an active metabolic organ and a key physiological regulator.

Identification of biomarkers for cardiac stress in patients is an important field of research for early diagnosis of diabetic cardiomyopathies. Our study thus provides a promising repertoire of cardiokines in fly that may prompt research on their orthologues in mammals.

MATERIALS AND METHODS

Fly husbandry and stocks

All lines were reared in incubator at 18°C for husbandry on reference food (ND, normal diet) and in incubators (light/dark cycle of 12/12h, humidity of 50%), at 23°C or 25°C for experiments in selected food as indicated. Animals were reared on normal diet (ND) at 25°C (or 23°C) containing per liter: 10g agar, 70g corn flour, 70g inactivated yeast extract and 3,75g Moldex (in Ethanol). High sugar diet (HSD) corresponds to the same food supplemented with 30% sucrose and high fat diet (HFD) with 30% coconut oil. For the purpose of experiments, flies were kept on ND or HSD at 25°C for 7 days then transferred at 23°C on ND, HSD or HFD for 3 more days.

The following lines were obtained from the BDSC: w^{1118} (BDSC#3605; RRID:BDSC_3605); *Dot-GAL4* (BDSC#67608; RRID:BDSC_67608); *tinC-Gal4.Delta4* (BDSC#92965; RRID:BDSC_92965); *UAS-GFP.Val10* (control for TRIP lines: *controlGFP*; BDSC#35786; RRID:BDSC_35786).

The following UAS-RNAi lines were obtained from the VDRC (RRID:SCR_013805): control lines #60100 (VDRC#60100, for KK lines) and #60000 (VDRC#60000, for GD lines); *UAS-gnmtKK* (VDRC#110623); *UAS-SardhKK* (VDRC#108873); *UAS-Snmp1KK* (VDRC#104210); *UAS-CG10960GD* (VDRC#8359); *UAS.CG34357KK* (VDRC#105185); *UAS-GILT2KK* (VDRC#104414); *UAS-CG3513KK* (VDRC#107668); *UAS-ImpL2KK* (VDRC#106543); *UAS-phuKK* (VDRC#100052); *UAS-Yp2GD* (VDRC#50156); *UAS-CG7997GD* (VDRC#16840); *UAS-Nepl10GD* (VDRC#7736); *UAS-InvadolysinGD* (VDRC#16416); *UAS-fitKK* (VDRC#109482); *UAS-fitGD* (VDRC#14434).

Other lines: $Hand^{4.2}$*-Gal4* (gift from Dr Achim Paululat, University of Osnabrück, Germany); $Hand^{4.2}$*-GAL4;R94C02::tdTomato* and *tinC-Gal4.Delta4;R94C02::tdTomato* (gift from Dr Karen Ocorr, SBP Medical Discovery Institute, San Diego, USA); *Dot-Gal4;R94C02::tdTomato* (this study); *Lsp2-Gal4* (gift from Dr Pierre Léopold, Institut Curie, Paris, France); *Lsp2-Gal4;R94C02::tdTomato* (this study); UAS-*fit*.3XHA (FlyORF#F002469; RRID: FlyBase_FBst0501830) called UAS-fit^{WT} in this study.

RNA extraction and sequencing

Progeny from w1118 line was obtained from calibrated tubes (20 females and 5 males per tube) at 25°C. Flies were reared on ND and HSD at 25°C for 7 days (20 females and 5 males per tube; males removed after 2 days; tubes are changed every 2 days). Mated females were then transferred at 23°C in order to get one tube of 20 females on ND, HSD and HFD per date. Three independent samples were collected at three different days for each food condition. For each sample, hearts of 30 females of each condition were dissected and immediately put in a collection tube containing 100ul of TRIzol (ThermoFisher Scientific, #15596026). RNA extraction was performed as described in [54]. RNA quantification was performed on Nanodrop (DS-11FX, DeNoviX Inc.) and Qubit (Invitrogen). The RNA-sequencing was performed on three independent samples (containing each >500ng) for each food condition. cDNA librairies were constructed and paired-end 50/30 illumina sequencing realized (NextSeq-500; TAGC/TGML core facility,

https://tagc.univ-amu.fr/en/resources/transcriptomic-genomic-platform-marseille-luminy).

Data analysis

Reads primo-analysis show that 90% are aligned on *Drosophila* genome reference Dm3. Quality control of the data was performed with FastQC v0.11.7 (available online http://www.bioinformatics.babraham.ac.uk/projects/fastqc/). The following tools were used to analyse the raw data: trimming was realized with Sickle (v1.33; https://github.com/najoshi/sickle; Joshi, N.A.; Fass, J.N., 2011); mapping on Dm3 genome release with Subread aligner (subread-align with subread v1.6.1[56]); Read counts with featureCounts (with subread v1.6.1[57]). Normalization of reads was implemented in Dseq2 and edgeR Bioconductor packages (RLE for DESeq2 and TMM for edgeR) [21,22]. Differentially Expressed Genes (DEG) was calculated in three conditions HSD vs ND, HFD vs ND and HSD vs HFD. Genes with a differential expression ≥1.5 in fold change and with a p-value <0.05 in both methods were selected.

Clustering of the datasets was performed using the unsupervised K-means learning algorithm and heatmaps realized with "pheatmap" v1.0.12 (https://rdocumentation.org/packages/pheatmap/versions/1.0.12) and "ComplexHeatmap"v 2.12.0 (available from the Bioconductor project: http://www.bioconductor.org/packages/devel/bioc/html/ComplexHeatmap.html Gu et al., 2016) packages in R/Rstudio (RStudio Team (2022). RStudio: Integrated Development Environment for R. RStudio, PBC, Boston, MA; URL: http://www.rstudio.com/); R project version 3.5.1 (RRID:SCR_001905). Validation of gene_id was performed with FlyBase ID validator tool (http://flybase.org/convert/id) in Dm6 genome annotation (Flybase: RRID:SCR_006549).

Functional annotation and sequence analysis

Functional annotation was performed using g:Profiler public resource (https://biit.cs.ut.ee/gprofiler/gost, RRID:SCR_006809) [33]. The complete list of TRUE significative DEG for each nutritional context was submitted as a query for "only annotated genes"; Benjamini-Hochberg FDR was chosen for the significance threshold filtering of enrichment terms (p=0.05) and search was run "Gene Ontology" databases (GO MP, GO BP, GO CC).

Prediction of signal peptides in the candidate genes sequences was done with BioMart on Ensembl project (https://www.ensembl.org/biomart/martview/, Ensembl RRID:SCR_002344). Query was performed on the BDGP6.2 *Drosophila* gene dataset on complete list of DEG for each condition (using the gene stable ID FBgnxxxx as a filter) and cleavage site (Signalp) was evaluated as a result. Enrichment map of KEGG pathways were realized using PANGEA[23] v1 beta 1 (https://www.flyrnai.org/tools/pangea/web/home/7227) with "KEGG pathways" as a proxy .

Fly heart live recording

Heart wall videos were performed on anaesthetized females expressing the *R94C02::tdTomato* transgene. 10 days old adult females are anaesthetized with FlyNap (Sordalab, #FLYNAP). Flies are then glued on a coverslip, on the dorsal side, in droplets of UV-curing glue (Norland Optical, #NOA61). After polymerization, the coverslip is fixed on a small petri dish, the dorsal side of the flies facing the 20x dry objective on a Zeiss Axioplan microscope. Cardiac activity is recorded in the A2-A3 abdominal region of the heart tube with a HD/high-speed camera (OrcaFlash4.0 digital CMOS camera, Hamamatsu Photonics). A 5sec movie at 300 frames/sec is recorded using HCI imaging software (Hamamatsu Photonics). Movies are analyzed with a designed R/Rstudio script (https://github.com/gvogler/FlyHearts-tdtK-Rscripts)[19], allowing the generation of M-modes and the quantification of different cardiac phenotypes. Cardiac parameters were calculated as below: Diastolic interval (DI) is the duration for each heart relaxation phase (diastole). Systolic interval (SI) is the duration of the contraction phase of the heart. Heart period (HP) is the time between the two consecutive diastoles (i.e., DI+SI) and heart rate is calculated from HP (1/HP). Arrhythmia index (AI) is the standard deviation of the HP mean for each fly normalized to the median HP. Fractional shortening was calculated as (diastolic diameter – systolic diameter)/diastolic diameter). Values were normalized to controls/date of experiment (gitlab.com/krifa_sallouha/TDTK_Data_AnalysisScripts).

Feeding behavior

10 days old adult females were starved overnight on PBS/Agarose vials. They were then challenged for 3 hours on tubes containing ND supplemented with 0.5% Erioglaucine disodium salt (Sigma Aldrich, #861146). Flies were frozen as group of 10/1.5ml Eppendorf tube until OD measurements at 629nm as described previously [59].

Western-blotting

Hemolymph samples from 20 females/lane, reared on ND, were extracted as described in [60], and prepared for Western Blotting. Hand/*control* and Hand/fit^{WT} were tested. The experiment was performed 3 times independently. cv-d was used as a normalizer for hemolymph proteins [61].

Proteins were resolved by SDS-PAGE, using 4-12% gradient gels (NuPage Novex Gel, InVitrogen #NP0335). Primary antibodies used were: rat anti-HA (1:1000, Merck/Roche, #ROAHAHA, RRID:AB_2687407) and guinea-pig anti-Cv-d (1:2000 [61], gift from Eaton lab). Membranes were washed in PBS tween 0,1% and incubated with secondary antibodies in this buffer for 2 hrs at room temperature. The following HRP conjugate secondary antibodies were used (Thermo Fisher Scientific): Goat anti-rat (1:2500, #A-10549, RRID:AB_10561556) and anti-guinea pig (1:2500, #A-

18769, RRID:AB_2535546). Chemiluminescence was observed using the ECL plus detection substrate kit (Thermo Fisher Scientific #32134). Images were generated using Fiji[62] (ImageJ version 2.0.0-RC-69/1.52n; RRID:SCR_002285).

Immunostaining

Adult brains were dissected in cold PBS on ice, fixed in 3,7% methanol-free formaldehyde (Polysciences Inc., #18814-10) for 25 min, washed several times in PBS + 0,1% Triton X-100 (PBT) before 2 hrs blocking in PBT containing 10% BSA. Primary antibody, Rabbit anti-Dilp5 (1:500, generated in Leopold's lab)[63] was incubated overnight at 4ºC. Alexa conjugated secondary antibody (Alexa Fluor 546 goat anti-rabbit: #A-11035, RRID:AB_143051) was incubated 2 hrs at room temperature. After several washes, brains were mounted in Vectashield (Eurobio scientific, #H1000-10). Fluorescence images were acquired using a Zeiss LSM780 (63x immersion objective) and processed with Fiji[62] (ImageJ version 2.0.0-RC-69/1.52n; RRID:SCR_002285).

Antibody staining quantification

For quantification, stacks were taken for the whole IPCs cluster in each brain, from top to bottom limit of the staining. Slices of the whole stack were used to evaluate the fluorescence intensity using Fiji[62] (StagReg, Time Series Analyser V3.0 and Roi Manager plugins). For each cluster, 3-4 individual neurons per cluster were measured as described previously[64].

Statistical analysis and Figures design

Statistical analyses and graphical representations were performed with Graphpad Prism V10 (© 2024 GraphPad Software; RRID:SCR_002798). The statistical test used for each experiment and the *P* values are indicated in the corresponding Figure and Figure legends. Fiji (ImageJ version 2.0.0-RC-69/1.52n; RRID:SCR_002285) was used for Image treatment from microscopy and Western Blotting. Affinity Designer v.1.10.8 (Serif, Europe; RRID:SCR_016952) was used for Figures elaboration.

Data availability

RNA-seq raw data have been deposited in the NCBI Gene Expression Omnibus (accession no.GSE235313) (RRID:SCR_005012).

Acknowledgments

We thank Dr Pauline Brochet for her help with GEO submission, Frederic Gallardo and Tahagan Titus for their technical assistance in fly food cooking. Charis Aubert, Alice Corbet and Loïc Crespo participated to the project during their internship. We thank the TGML sequencing platform. We

thank E. Castellani from the IBDM Imaging Facility and France Bio-Imaging infrastructure - ANR-10 INBS-04-01. We thank the Bloomington Stock Center and the Vienna *Drosophila* RNAi Center for fly stocks.

Funding is from Amidex (grant n°AMX-21-PEP-020 to N.A.), ANR (grant n°ANR-22-CE17-0051-03 to N.A.), Fondation de France (grant n°00071034 to L.P.), Inserm and Aix-Marseille University (AMU).

Contributions

Conceptualization: L.P., N.A., Data Curation: L.K.C., L.K., Formal Analysis: L.K.C, L.K., N.A., Methodology: N.A., S.K., L.P., Experimental Investigation: N.A., L.K., M.T., C.A., L.C., A.C., L.R., Project Administration: N.A., L.P., L.R., Supervision; N.A., Validation: N.A., Visualization: N.A., Writing- Original Draft Preparation: N.A., L.P., Writing- Review & Editing: N.A.

References

1. Saeedi, P. *et al.* Global and regional diabetes prevalence estimates for 2019 and projections for 2030 and 2045: Results from the International Diabetes Federation Diabetes Atlas, 9th edition. *Diabetes Res. Clin. Pract.* **157**, 107843 (2019).
2. Tan, Y. *et al.* Mechanisms of diabetic cardiomyopathy and potential therapeutic strategies: preclinical and clinical evidence. *Nat. Rev. Cardiol.* **17**, 585–607 (2020).
3. Borghetti, G. *et al.* Diabetic Cardiomyopathy: Current and Future Therapies. Beyond Glycemic Control. *Front. Physiol.* **9**, 1514 (2018).
4. Bier, E. & Bodmer, R. Drosophila, an emerging model for cardiac disease. *Gene* **342**, 1–11 (2004).
5. Blice-Baum, A. C. *et al.* As time flies by: Investigating cardiac aging in the short-lived Drosophila model. *Biochim. Biophys. Acta BBA - Mol. Basis Dis.* **1865**, 1831–1844 (2019).
6. Ocorr, K. *et al.* Genetic control of heart function and aging in Drosophila. *Trends Cardiovasc. Med.* **17**, 177–182 (2007).
7. Saha, S. *et al.* Genetic architecture of natural variation of cardiac performance in flies. 2021.06.08.447524 Preprint at https://doi.org/10.1101/2021.06.08.447524 (2022).
8. Alfa, R. W. & Kim, S. K. Using Drosophila to discover mechanisms underlying type 2 diabetes. *Dis. Model. Mech.* **9**, 365–376 (2016).
9. Diop, S. B. & Bodmer, R. Gaining Insights into Diabetic Cardiomyopathy from Drosophila. *Trends Endocrinol. Metab.* **26**, 618–627 (2015).
10. Rotstein, B. & Paululat, A. On the Morphology of the Drosophila Heart. *J. Cardiovasc. Dev. Dis.* **3**, 15 (2016).
11. Kawasaki, Y. *et al.* Three-dimensional architecture of pericardial nephrocytes in Drosophila melanogaster revealed by FIB/SEM tomography. *Cell Tissue Res.* **378**, 289–300 (2019).
12. Lim, H.-Y., Wang, W., Chen, J., Ocorr, K. & Bodmer, R. ROS Regulate Cardiac Function via a Distinct Paracrine Mechanism. *Cell Rep.* **7**, 35–44 (2014).
13. Na, J. *et al.* A Drosophila Model of High Sugar Diet-Induced Cardiomyopathy. *PLoS Genet.* **9**, e1003175 (2013).
14. Birse, R. T. *et al.* High-Fat-Diet-Induced Obesity and Heart Dysfunction Are Regulated by the TOR Pathway in Drosophila. *Cell Metab.* **12**, 533–544 (2010).

15. Diop, S. *et al.* PGC-1/spargel counteracts High-fat-diet-induced obesity and cardiac lipotoxicity downstream of TOR and brummer ATGL lipase. *Cell Rep.* **10**, 1572–1584 (2015).
16. Liu, P., Chang, K., Requejo, G. & Bai, H. mTORC2 protects the heart from high-fat diet-induced cardiomyopathy through mitochondrial fission in Drosophila. *Front. Cell Dev. Biol.* **10**, 866210 (2022).
17. Sun, J. *et al.* Drosophila FIT is a protein-specific satiety hormone essential for feeding control. *Nat. Commun.* **8**, 1–13 (2017).
18. Klassen, M. P. *et al.* Age-dependent diastolic heart failure in an in vivo Drosophila model. *eLife* **6**, e20851 (2017).
19. Vogler, G. gvogler/FlyHearts-tdtK-Rscripts: First release of the R tdtK script. Zenodo https://doi.org/10.5281/zenodo.4749935 (2021).
20. Fink, M. *et al.* A new method for detection and quantification of heartbeat parameters in Drosophila, zebrafish, and embryonic mouse hearts. *BioTechniques* **46**, 101–113 (2009).
21. Love, M. I., Huber, W. & Anders, S. Moderated estimation of fold change and dispersion for RNA-seq data with DESeq2. *Genome Biol.* **15**, 550 (2014).
22. McCarthy, D. J., Chen, Y. & Smyth, G. K. Differential expression analysis of multifactor RNA-Seq experiments with respect to biological variation. *Nucleic Acids Res.* **40**, 4288–4297 (2012).
23. Hu, Y. *et al.* PANGEA: a new gene set enrichment tool for Drosophila and common research organisms. *Nucleic Acids Res.* **51**, W419–W426 (2023).
24. Hu, Y. *et al.* FlyRNAi.org—the database of the Drosophila RNAi screening center and transgenic RNAi project: 2021 update. *Nucleic Acids Res.* **49**, D908–D915 (2021).
25. Salway, J. G. *Metabolism at a Glance*. (John Wiley & Sons, 2017).
26. Ducker, G. S. & Rabinowitz, J. D. One-Carbon Metabolism in Health and Disease. *Cell Metab.* **25**, 27–42 (2017).
27. Li, H. *et al. Fly Cell Atlas: A Single-Cell Transcriptomic Atlas of the Adult Fruit Fly*. http://biorxiv.org/lookup/doi/10.1101/2021.07.04.451050 (2021) doi:10.1101/2021.07.04.451050.
28. Lee, T. E., Yu, L., Wolf, M. J. & Rockman, H. A. Galactokinase Is a Novel Modifier of Calcineurin-Induced Cardiomyopathy in *Drosophila*. *Genetics* **198**, 591–603 (2014).
29. Talamillo, A. *et al.* Scavenger Receptors Mediate the Role of SUMO and Ftz-f1 in Drosophila Steroidogenesis. *PLoS Genet.* **9**, e1003473 (2013).
30. Tan, Y. *et al.* Mechanisms of diabetic cardiomyopathy and potential therapeutic strategies: preclinical and clinical evidence. *Nat. Rev. Cardiol.* **17**, 585–607 (2020).
31. Maria, Z., Campolo, A. R. & Lacombe, V. A. Diabetes Alters the Expression and Translocation of the Insulin-Sensitive Glucose Transporters 4 and 8 in the Atria. *PloS One* **10**, e0146033 (2015).
32. Havula, E. *et al.* Genetic variation of macronutrient tolerance in Drosophila melanogaster. *Nat. Commun.* **13**, 1637 (2022).
33. Raudvere, U. *et al.* g:Profiler: a web server for functional enrichment analysis and conversions of gene lists (2019 update). *Nucleic Acids Res.* **47**, W191–W198 (2019).
34. Martin, F. J. *et al.* Ensembl 2023. *Nucleic Acids Res.* **51**, D933–D941 (2023).
35. Nielsen, H., Tsirigos, K. D., Brunak, S. & von Heijne, G. A Brief History of Protein Sorting Prediction. *Protein J.* **38**, 200–216 (2019).
36. Brogiolo, W. *et al.* An evolutionarily conserved function of the drosophila insulin receptor and insulin-like peptides in growth control. *Curr. Biol.* **11**, 213–221 (2001).
37. Géminard, C., Rulifson, E. J. & Léopold, P. Remote Control of Insulin Secretion by Fat Cells in Drosophila. *Cell Metab.* **10**, 199–207 (2009).
38. Obata, F. & Miura, M. Enhancing S-adenosyl-methionine catabolism extends Drosophila lifespan. *Nat. Commun.* **6**, 1–9 (2015).
39. Xiao, Y. *et al.* Role of S-adenosylhomocysteine in cardiovascular disease and its potential epigenetic mechanism. *Int. J. Biochem. Cell Biol.* **67**, 158–166 (2015).
40. Wittemans, L. B. L. *et al.* Assessing the causal association of glycine with risk of cardio-metabolic diseases. *Nat. Commun.* **10**, 1060 (2019).
41. Daenzer, J. M. I. *et al.* Acute and long-term outcomes in a Drosophila melanogaster model of classic galactosemia occur independently of galactose-1-phosphate accumulation. *Dis. Model. Mech.*

9, 1375–1382 (2016).
42. Maria, Z., Campolo, A. R., Scherlag, B. J., Ritchey, J. W. & Lacombe, V. A. Dysregulation of insulin-sensitive glucose transporters during insulin resistance-induced atrial fibrillation. *Biochim. Biophys. Acta BBA - Mol. Basis Dis.* **1864**, 987–996 (2018).
43. Honegger, B. *et al.* Imp-L2, a putative homolog of vertebrate IGF-binding protein 7, counteracts insulin signaling in Drosophila and is essential for starvation resistance. *J. Biol.* **7**, 10 (2008).
44. Arquier, N. *et al.* Drosophila ALS Regulates Growth and Metabolism through Functional Interaction with Insulin-Like Peptides. *Cell Metab.* **7**, 333–338 (2008).
45. Kwon, Y. *et al.* Systemic organ wasting induced by localized expression of the secreted Insulin/IGF antagonist ImpL2. *Dev. Cell* **33**, 36–47 (2015).
46. Figueroa-Clarevega, A. & Bilder, D. Malignant drosophila tumors interrupt insulin signaling to induce cachexia-like wasting. *Dev. Cell* **33**, 47–56 (2015).
47. Carvalho-Santos, Z. *et al.* Cellular metabolic reprogramming controls sugar appetite in Drosophila. *Nat. Metab.* **2**, 958–973 (2020).
48. Al-Mohanna, F. The Cardiokines. in *Endocrinology of the Heart in Health and Disease* 87–114 (Elsevier, 2017). doi:10.1016/B978-0-12-803111-7.00004-X.
49. Planavila, A., Fernández-Solà, J. & Villarroya, F. Cardiokines as Modulators of Stress-Induced Cardiac Disorders. in *Advances in Protein Chemistry and Structural Biology* vol. 108 227–256 (Elsevier, 2017).
50. Wu, Y.-S., Zhu, B., Luo, A.-L., Yang, L. & Yang, C. The Role of Cardiokines in Heart Diseases: Beneficial or Detrimental? *BioMed Res. Int.* **2018**, 1–14 (2018).
51. Lee, J., Bassel-duby, R. & Olson, E. N. Heart- and muscle-derived signaling system dependent on MED13 and Wingless controls obesity in Drosophila. *Proc. Natl. Acad. Sci. U. S. A.* **111**, 9491–6 (2014).
52. Lee, S., Bao, H., Ishikawa, Z., Wang, W. & Lim, H. Y. Cardiomyocyte Regulation of Systemic Lipid Metabolism by the Apolipoprotein B-Containing Lipoproteins in Drosophila. *PLoS Genet.* **13**, 1–25 (2017).
53. Liu, Y., Bao, H., Wang, W. & Lim, H.-Y. Cardiac Snail family of transcription factors directs systemic lipid metabolism in Drosophila. *PLOS Genet.* **15**, e1008487 (2019).
54. Zeitouni, B. *et al.* Signalling pathways involved in adult heart formation revealed by gene expression profiling in Drosophila. *PLoS Genet.* **3**, 1907–1921 (2007).
55. Joshi, N.A.; Fass, J.N. Sickle: A sliding-window, adaptive, quality-based trimming tool for FastQ files (Version 1.33) [Software]. (2011).
56. Liao, Y., Smyth, G. K. & Shi, W. The Subread aligner: fast, accurate and scalable read mapping by seed-and-vote. *Nucleic Acids Res.* **41**, e108 (2013).
57. Liao, Y., Smyth, G. K. & Shi, W. featureCounts: an efficient general purpose program for assigning sequence reads to genomic features. *Bioinforma. Oxf. Engl.* **30**, 923–930 (2014).
58. Gu, Z., Eils, R. & Schlesner, M. Complex heatmaps reveal patterns and correlations in multidimensional genomic data. *Bioinforma. Oxf. Engl.* **32**, 2847–2849 (2016).
59. Bjordal, M., Arquier, N., Kniazeff, J., Pin, J. P. & Léopold, P. Sensing of amino acids in a dopaminergic circuitry promotes rejection of an incomplete diet in drosophila. *Cell* **156**, 510–521 (2014).
60. Damrau, C. & Members, B. lab. Haemolymph extraction of adult Drosophila. (2015).
61. Palm, W. *et al.* Lipoproteins in Drosophila melanogaster-assembly, function, and influence on tissue lipid composition. *PLoS Genet.* **8**, e1002828 (2012).
62. Schindelin, J. *et al.* Fiji: An open-source platform for biological-image analysis. *Nat. Methods* **9**, 676–682 (2012).
63. Géminard, C., Rulifson, E. J. & Léopold, P. Remote Control of Insulin Secretion by Fat Cells in Drosophila. *Cell Metab.* **10**, 199–207 (2009).
64. Arquier, N., Bjordal, M., Hammann, P., Kuhn, L. & Léopold, P. Brain adiponectin signaling controls peripheral insulin response in Drosophila. *Nat. Commun.* **12**, 5633 (2021).

65. Frasch, M. Genome-Wide Approaches to Drosophila Heart Development. *J. Cardiovasc. Dev. Dis.* **3**, 20 (2016).

Legends to Figures

Figure 1. Cardiac performances measured in control flies in response to diets. (A) Live imaging was performed on anesthetized Females (see Methods) expressing the tdTomato (tdTk) reporter in cardiomyocytes. Analysis generated M-Modes (DI=Diastolic Interval; SI=Systolic Interval; HP=Heart Period; EDD=End Diastolic Diameter; ESD=End Systolic Diameter). (B-J) Measurements of cardiac parameters form Hand>*controlKK* challenged 10days in ND, HSD or 3 days in HFD. (B-E) Box plots showing normalized values for rhythmicity (HP, DI, SI) and associated phenotypes (AI). (F-H) Box plots showing normalized values for structural (ESD, EDD) and associated phenotypes (FS). (I-J) Box plots showing normalized values for volumetric hemolymph estimation in the heart (SV, CO). ND, white plots; HSD, blue plots; HFD, yellow plots. Numbers corresponds to the individual flies co-evaluated in each diet. Statistical significance was tested using Krustal-Wallis with Dunn's multiple comparisons test. *P* values are indicated.

Figure 2. Feeding High fat or high sugar impacts cardiac metabolic regulations. (A) Scheme of the protocol used for batch RNAseq analysis of HFD/HSD-induced cardiac transcriptome modifications. (B,C) Volcano plots showing deregulated genes in HSD and HFD (red numbers) .Blue dots indicate genes with an absolute Fold Change ≥0.585 and adjusted *P* value <0.05. Selected hits are indicated. (D) Venn diagram of DEG identified in the three conditions (padj<0.05). (E,F) Heat maps showing unsupervised clustering analysis and resulting Log2(FC) expression plots for the 75 (E) and the 35 (F) common DEG identified in HSD and HFD stresses (padj<0.05). (G,I) Network graphs obtained with PANGEA enrichment tool for of HSD (G) or HFD (I) DEG. Circle nodes correspond to genes, triangle nodes represent KEGG pathways while edges represent gene to gene association. (H,J) Bar graphs showing log2FC enrichment values for KEGG pathways annotations in PANGEA (padj<0.05).

Figure 3. Cardiac function of Glycine metabolism and metabolite transporters. (A) Scheme representing the Glycine cycle, part of the 1C-metabolism pathway. Conversion of Glycine to Sarcosine by GNMT (reversal conversion by SARDH) allows transfer of methyl-group from the universal donor SAM (S-adenosylmethionine) to several cellular components, leading to the formation of S-adenosylhomocysteine (SAH). (B) Z-projection images of Hand>*GnmtKK* (KD) and >*controlKK* heart imaging and generated M-modes in ND and HSD. (C) Effect of *Gnmt* and *Sardh* knockdown (KD) on ESD under ND (white box plots) or HSD (blue box plots) compared to controls. (D) HP, (E) AI and (F) FS defects following *Gnmt* KD compared to control in HSD. (G) Schematic

representation of Leloir pathway, comprising enzymes involved in Galactose catabolism. b-Galactose is converted in a-Galactose by CG32444/Galm1, then in Galactose-1P by *Galk*. Following steps lead to Glucose-1P production. Enzymes in grey (Galt and Gale) were not identified in our transcriptomic analysis. (H) Z-projection images of Hand>*GalkTRIP* (KD) and *>controlTRIP* heart imaging and generated M-modes in ND and HSD. (I) HP and (J) DI defects following *Galk* KD in ND (white box plots) and in HSD (blue box plots compared to controls. (K) Z-projection images of Hand>*Snmp1KK* (KD), *>Snmp1*^{WT} (OE), with respective controls heart imaging and generated M-modes in ND. Dysfunctional ostia are observed upon *Snmp1*^{WT} OE (white star). (L) Defects in EDD and (M) FS upon *Snmp1* KD and OE in ND compared to controls. (N) Z-projection images of Hand>*nebuGD* (KD) and *>controlGD* heart imaging and generated M-modes in ND and HFD. (O) ESD and (P) EDD defects following *nebu* KD in ND (white) and HFD (yellow) compared to controls. Values where normalized to controls. The number of individuals analyzed in each condition (genotype/diet) is indicated. Statistical significance was tested using Krustal-Wallis with Dunn's multiple comparisons test. Significant *P* values are indicated.

Figure 4. Cardiac function of newly identified cardiokines. (A) Table showing selected putative cardiokine genes identified in HSD and HFD. Fly gene name and Flybase ID (column 1), HSD and HFD dysregulations observed (column 2), best human orthologue (column 3) based on DIOPT score (column 4), HuGE score for diabetes and cardiovascular diseases (quantification of genetic association of genes to diseases based on human GWAS analysis; column 5), protein class and blood detection (Human protein atlas, column 6), identified cardiac phenotypes in fly (column 7). (B) HP, (C) FS and (D) SI modifications observed in Hand> driven KD (grey) compared to respective controls (red). (E) EDD modifications in Hand> driven *phu* KD (grey) compared to control (red). Values where normalized to controls. The number of individuals analyzed in each condition (genotype/diet) is indicated. Statistical significance was tested using Krustal-Wallis with Dunn's multiple comparisons test. Significant *P* values are indicated.

Genotypes: UAS-*CG34357KK*, UAS-*GILT2KK*, UAS-*CG3513KK*, UAS-*Yp2GD*, UAS-*CG7997GD*, UAS-*Nepl10*, UAS-*phuKK*, UAS-*ImpL2KK*.

Figure 5. Cardiac Fit is required for cardiac rhythm modulation. (A-C) Effects of *fit* KD (*fitKK*) and OE (*fit*^{WT}) on HP. *fit* expression was manipulated in the whole heart (A), in cardiomyocytes (B) and in pericardial cells (C) and compared to respective control flies in ND. (D) AI modification in *fit* KD induced in the whole heart (Hand>), in cardiomyocytes (tincD4>) and in pericardial cells (Dot>) compared to respective controls. (E) Effect of *fit* OE induced in fat body (Lsp2>) on HP compared to control in ND. (F) Effect of Hand> driven *fit* KD on HP compared to control in HSD. (G) Effect of Hand>

driven *fit* KD on ESD compared to control in HFD. Values were normalized to controls. The number of individuals analyzed in each condition (genotype/diet) is indicated. Statistical significance was tested using Krustal-Wallis with Dunn's multiple comparisons test. Significant *P* values are indicated.

Figure 6. Secreted cardiac Fit regulates food intake via Dilp release. Quantification of food intake in females overnight starved and refed 3 hours. (A) *fit* KD and *fit* OE (B) were induced in the whole heart (Hand>), in cardiomyocytes (tinCD4>) and in pericardial cells (Dot>) and compared to respective control flies. Values are normalized to controls. Each point corresponds to averaged values for 10 adults obtained from 3-6 independent experiments. Statistical significance was tested using ordinary two-way ANOVA with Sidak's multiple comparisons test. (C) Fit-HA immunodetection in hemolymph extracts from Hand> driven *fit* OE compared to controls. cv-d is a control for hemolymph proteins (n=3 independent experiments). *fit* OE (HA-tagged fit^{WT}). (D) Dilp5 immunostaining in IPCs on dissected adult brains at t0 (overnight starvation, left panels) and t3 (3hours refeeding ND, right panels). Genotypes: Hand> driven *fit* OE (fit^{WT}; light red) *fit* KD (*fitKK*; pink) and controls (dark red). (E) Quantification of fluorescence intensity in IPCs from to 3 normalized independent experiments related to (D). Values are normalized to each time control (t0: points; t3: triangles). Each point corresponds to 3-4 averaged measurements in each IPC. The number of individuals analyzed in each condition (genotype/time point) is indicated. Statistical significance was tested using ordinary two-way ANOVA with Sidak's multiple comparisons test. Significant *P* values are indicated. (F) Proposed working model of cardiac *fit* function in ND and in response to HSD and HFD. In ND, cardiac *fit* expression is autonomously regulating cardiac rate speed as well as preventing arrhythmias. Secreted Fit can remotely regulate food intake by modulating Dilp release from the IPCs. In HSD, reduced *fit* expression is sufficient to counteract the induced-decrease cardiac rate speed and to reduce arrhythmias. In HFD, cardiac hypertrophy tends to be rescued by decreased *fit* expression.

Figure S1. Cardiac performances measured in control flies in response to diets (related to Figure 1). Measurements of cardiac parameters form Hand>*controlGD* and Hand>*controlGFP* challenged 10days in ND, HSD or 3 days in HFD. (A-D) Box plots showing normalized values for rhythmicity (HP, DI, SI) and associated phenotypes (AI). (E-G) Box plots showing normalized values for structural (ESD, EDD) and associated phenotypes (FS). (H-I) Box plots showing normalized values for volumetric hemolymph estimation in the heart (SV, CO). ND, white plots; HSD, blue plots; HFD, yellow plots. Numbers corresponds to the individuals co-evaluated in each diet. Statistical significance was tested using Krustal-Wallis with Dunn's multiple comparisons test. Significant *P* values are indicated.

Figure S2. Comparative analysis of the transcriptome with DEseq2 and edgeR_TMM (related to Figure 2). (A-C) Compared analysis for HSD vs ND results. (D-F) Compared analysis for HFD vs ND results. (A,D) Venn diagrams of selected genes (padj. <0.05, FC>=1.5). After filtering, 9981 genes were analyzed with each method. Sugar or Fat hits in yellow and normal genes in blue. (B,E) Comparison of genes according to Log2FC (left panels) or padj. value (right panels) with each method. (C,F) Volcano plots showing the repartition of the total genes in each condition determined in DEseq2 *vs* edgeR_TMM. padj<0.05, abs(log2FC)>=0.585, blue crosses indicate significant hits *vs* grey n.s. (G) Volcano plot highlighting members of the 1C-metabolism pathway downregulated in HSD *vs* ND condition.

Figure S3 (related to Figure 3). Effect of Hand> driven knockdown (KD) of *Gnmt* (*GnmtKK*) and *Sardh* (*SardhKK*) on CO (A) and EDD (B) in ND (white box plots) or HSD (blue box plots). (C) Effect of Hand> driven *Gnmt* and *Sardh* KD on FS, (D) HP and (E) AI in ND. (F) Effect of Hand> driven *Snmp1* KD (*Snmp1KK*) and OE ($Snmp1^{WT}$) on ESD and (G) AI in ND (white box plots). (H) M-modes generated from cardiac imaging of Hand> driven *Snmp1* OE showing arrhythmic pattern compared to control (white stars). (I) Image capture from representative movies showing abdominal fat accumulation (arrowhead) in Hand> driven *Snmp1* KD and control in ND. (J) Effect of Hand> driven *nebu* KD (*nebuGD*) on HP, (K) DI and (L) SV compared to controls in ND (white box plots) and in HFD (yellow box plots). Values are normalized to controls. The number of individuals analyzed in each condition (genotype/diet) is indicated. Statistical significance was tested using Krustal-Wallis with Dunn's multiple comparisons test. Significant *P* values are indicated.

Figure S4 (related to Figure 4). (A) gProfiler graphical representation of enrichment analyses for cellular components GO terms on total DEG identified in HFD (yellow) and HSD (blue) *vs* ND. (B) Venn diagram of DEG identified with Biomart/SignalP 5.0 in HSD and HFD vs ND (padj<0.05). (C) DI and (D) ESD modifications in Hand> driven KD (grey) compared to respective controls (red). (E) Effect of Hand> driven *Invadolysin* KD on HP and (F) FS compared to control. Values where normalized to controls. The number of individuals analyzed in each condition (genotype/diet) is indicated. Statistical significance was tested using Krustal-Wallis with Dunn's multiple comparisons test. Significant *P* values are indicated.

Genotypes: UAS-*CG34357KK*, UAS-*GILT2KK*, UAS-*CG3513KK*, UAS-*Yp2GD*, UAS-*CG7997GD*, UAS-*Nepl10*, UAS-*InvadolysinGD*.

Figure S5 (related to Figure 5). (A) Diagram of the heart and its cell types with the specific Gal4 lines associated. Hand4.2-Gal4 is expressed in all cell types (whole heart), tinCDelta4-Gal4 in cardiomyocytes (red) and valve cells (brown), Dot-Gal4 in pericardial cells (beige); adapted from[65]. (B) Effects of Hand> driven *fit* KD (*fitKK*) on SI and (C) DI compared to control in ND (white plots) and HSD (blue plots). (D) Effects of Hand> driven *fit* KD (*fitGD*) on HP, (E) SI and (F) DI compared to control in ND (white plots) and HSD (blue plots). (G) AI modifications induced by Hand> driven *fit* knockdowns (*fitGD*) and (H) (*fitKK*) compared to respective controls in ND (white plots) and HSD (blue plots). Values were normalized to controls. The number of individuals analyzed in each condition (genotype/diet) is indicated. Statistical significance was tested using Krustal-Wallis with Dunn's multiple comparisons test. Significant *P* values are indicated.

Figure S6 (related to Figure 6). (G) Quantification of fluorescence intensity in IPCs from to 2 normalized independent experiments. Genotypes: Dot> driven *fit* OE (*fit*^{WT}; light red) *fit* KD *(fitKK;* pink) and controls (dark red). Values are normalized to each time control (t0: points; t3: triangles). Each point corresponds to 3-4 averaged measurements/IPC. The number of individuals analyzed in each condition (genotype/time point) is indicated. Statistical significance was tested using ordinary two-way ANOVA with Sidak's multiple comparisons test. Significant *P* values are indicated.

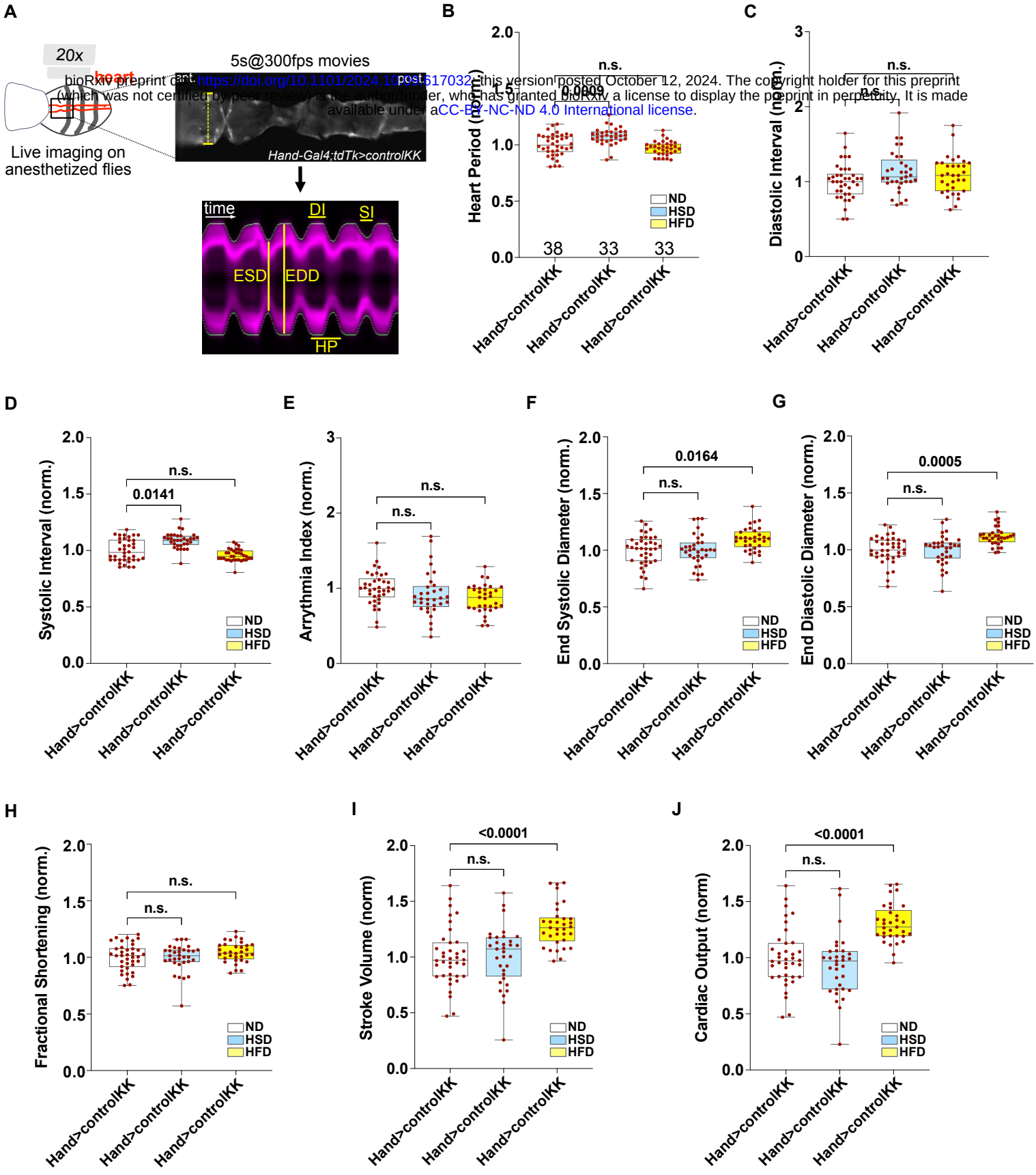

Figure 1

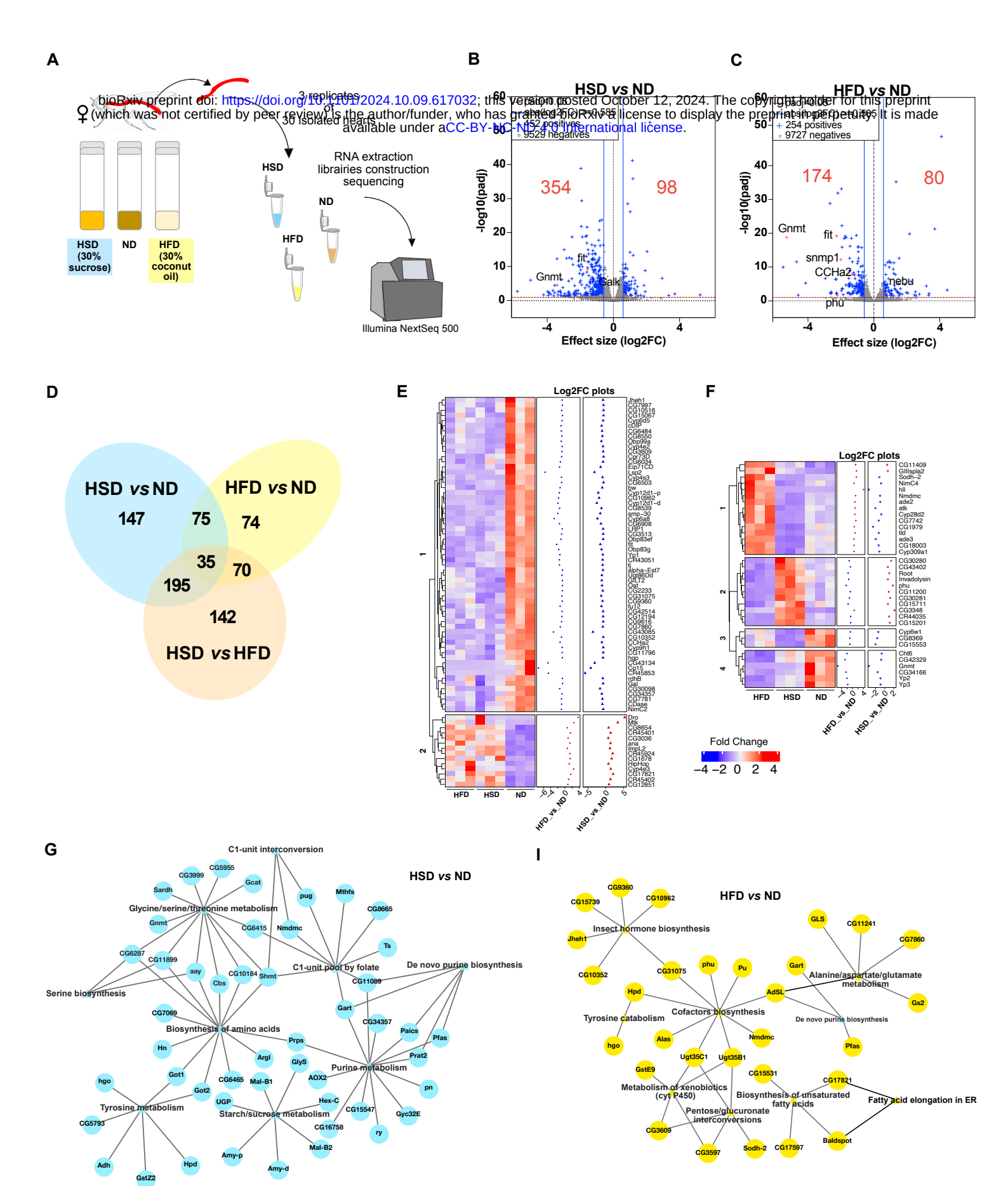

Figure 2

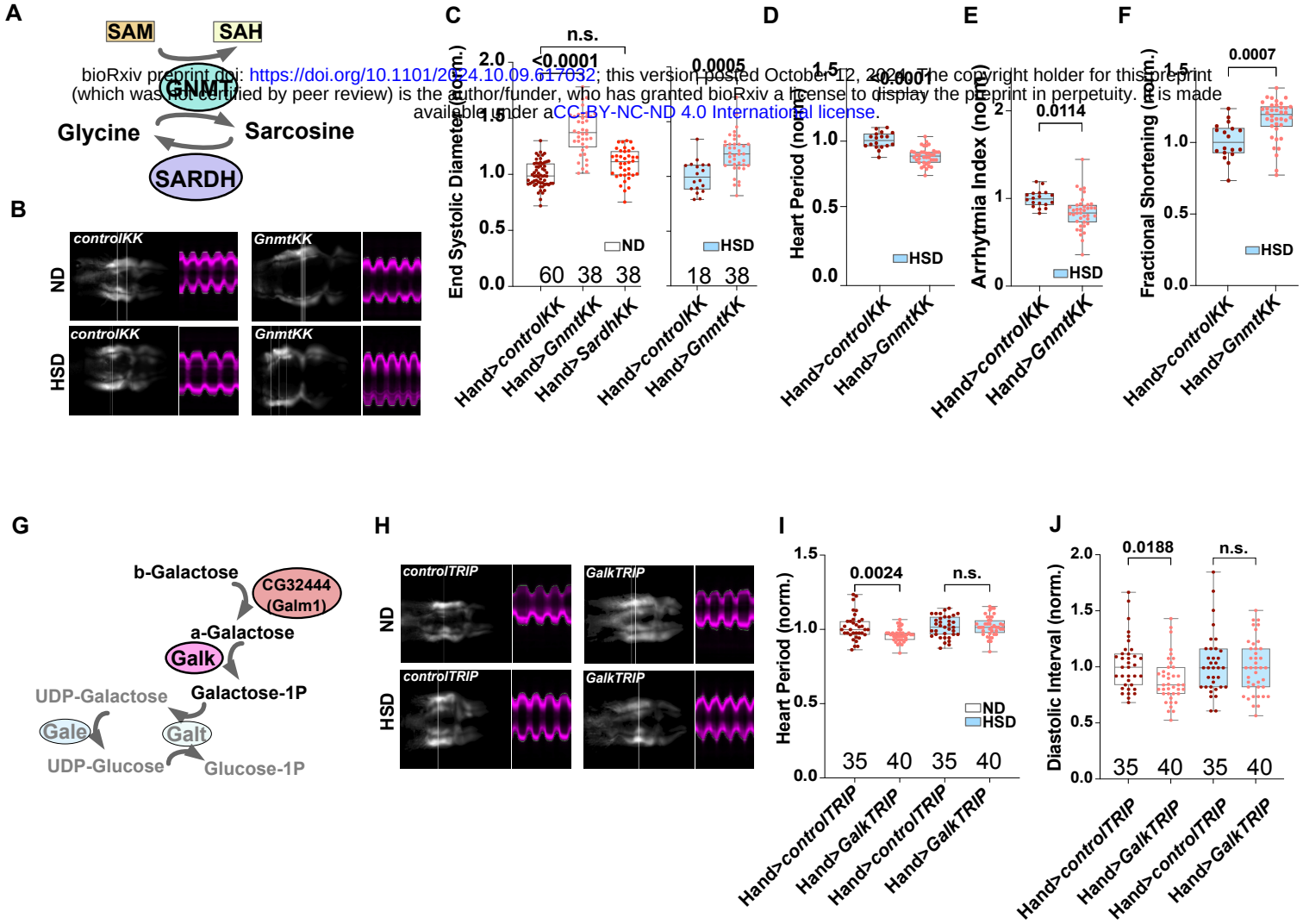

Figure 3

A

Drosophila gene (1)	DEG/diet	Human orthologue	DIOPT score (2)	CMD-KP annoted traits (HuGE score) (3)	Human Protein (4)	Cardiac phenotypes in flies (5)
phu (FBgn0034379)	HFD↓ HSD↑	ALPL	14	Plasma C-reactive protein (66.18: very strong) - Calcific aortic stenosis (45: very strong)	Candidate cardiovascular disease genes; Alkaline phosphatase; Metabolic proteins	EDD, HP, SI
Invadolysin (FBgn0086359)	HFD↓ HSD↑	LMLN	14	Resting heart rate (3: moderate)	Hydrolase; Metalloprotease	none
CG7997 (FBgn0034117)	HFD / HSD↓	NAGA	12	HDL cholesterol (45; very strong) - Calcium regulation (3; moderate)	Glycosidase; lipid metabolism; plasma proteins; detected in blood by MS	ESD, FS, HP, SI
CG34357 (FBgn0085386)	HFD / HSD↓	GUCY2D	9	Diastolic blood pressure (45; very strong) - Hypertension (3.32; moderate) - Systolic blood pressure (3; moderate)	guanylate cyclase; metabolic proteins	HP, SI, DI, AI
GILT2 (FBgn0039099)	HFD / HSD↓	IFI30	7	Diastolic blood pressure (3; moderate)	Lysosomal thiol reductase; localised to vesicules and detected in blood by MS	FS, HP, SI
Yp2 (FBgn0005391)	HFD / HSD↓	PNLIPRP3	4	Any cardiovascular disease (19.31; strong)	Hydrolase; lipid metabolism; secreted	ESD, FS, HP, SI
Nepl10 (FBgn0033742)	HFD / HSD↓	MME	4	Glycemia regulation (4.82 moderate) - Diastolic blood pressure (3; moderate) - Systolic blood pressure (3; moderate)	(degradation of ANF and BNF); Plasma proteins; detected in blood by MS	HP, SI, DI
		ECEL1	4	Obesity (50.09; very strong) - Diabetic retinopathy (7.42; moderate) - Heart rate (3; moderate)	M13 metalloprotease family; regulator of neuropeptides and peptide hormone activity	
CG3513 (FBgn0031559)	HFD / HSD↓	EPPIN	4	Abdominal aortic aneurysm (3: moderate) - Type 2 diabetes (2.76: anecdotal)	Pepetidase; secreted	HP, SI, DI
ImpL2 (FBgn0001257)	HFD / HSD↑	DSCAM	2	Plasma C-reactive protein (44.20: very strong) - Heart pulse (22.40: very strong)	Cell adhesion ; Plasma protein	HP, SI
		SDK2	2	Heart rate (45: very strong) - Heart pulse (45: very strong)	Cell adhesion	

(1) identified as putative encoding cardiokine in our study
(2) http://www.flyrnai.org/diopt
(3) Common Metabolic Disease - Knowledge Portal (https://md.hugeamp.org/); HuGE score quantify the genetic involvement of the gene disease based on GWAS data
(4) The Human protein atlas database (https://www.proteinatlas.org/)
(5) measured in our study

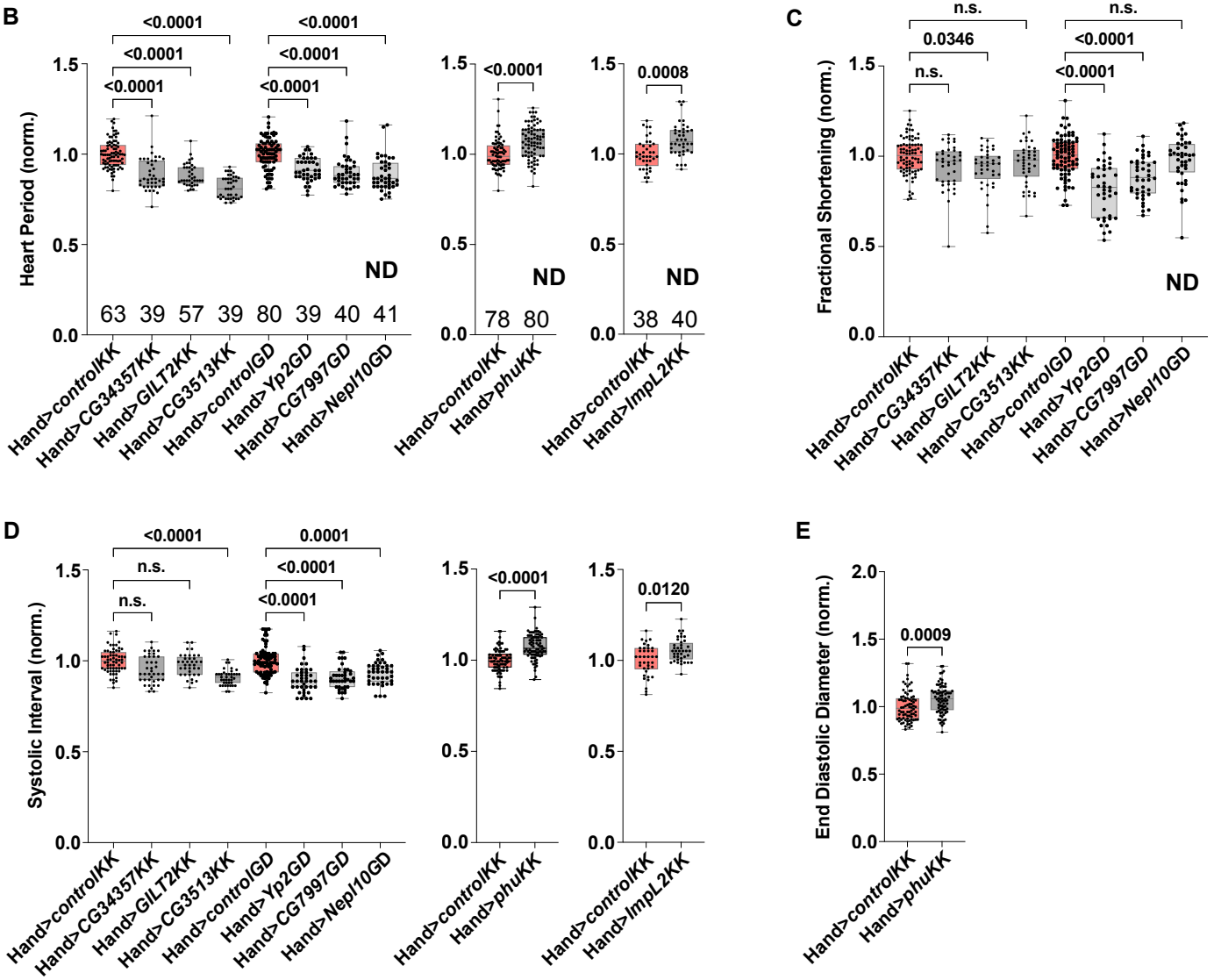

Figure 4

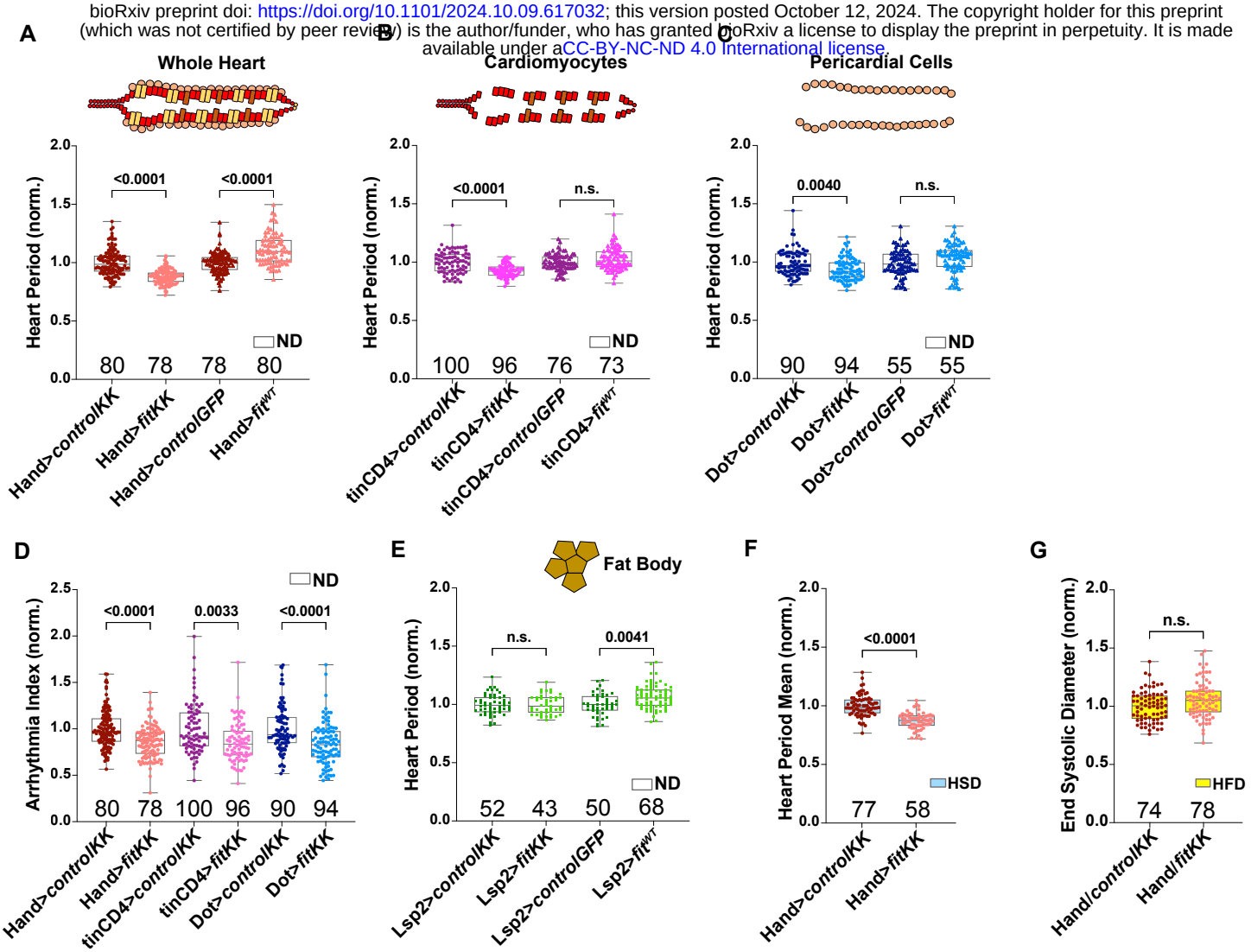

Figure 5

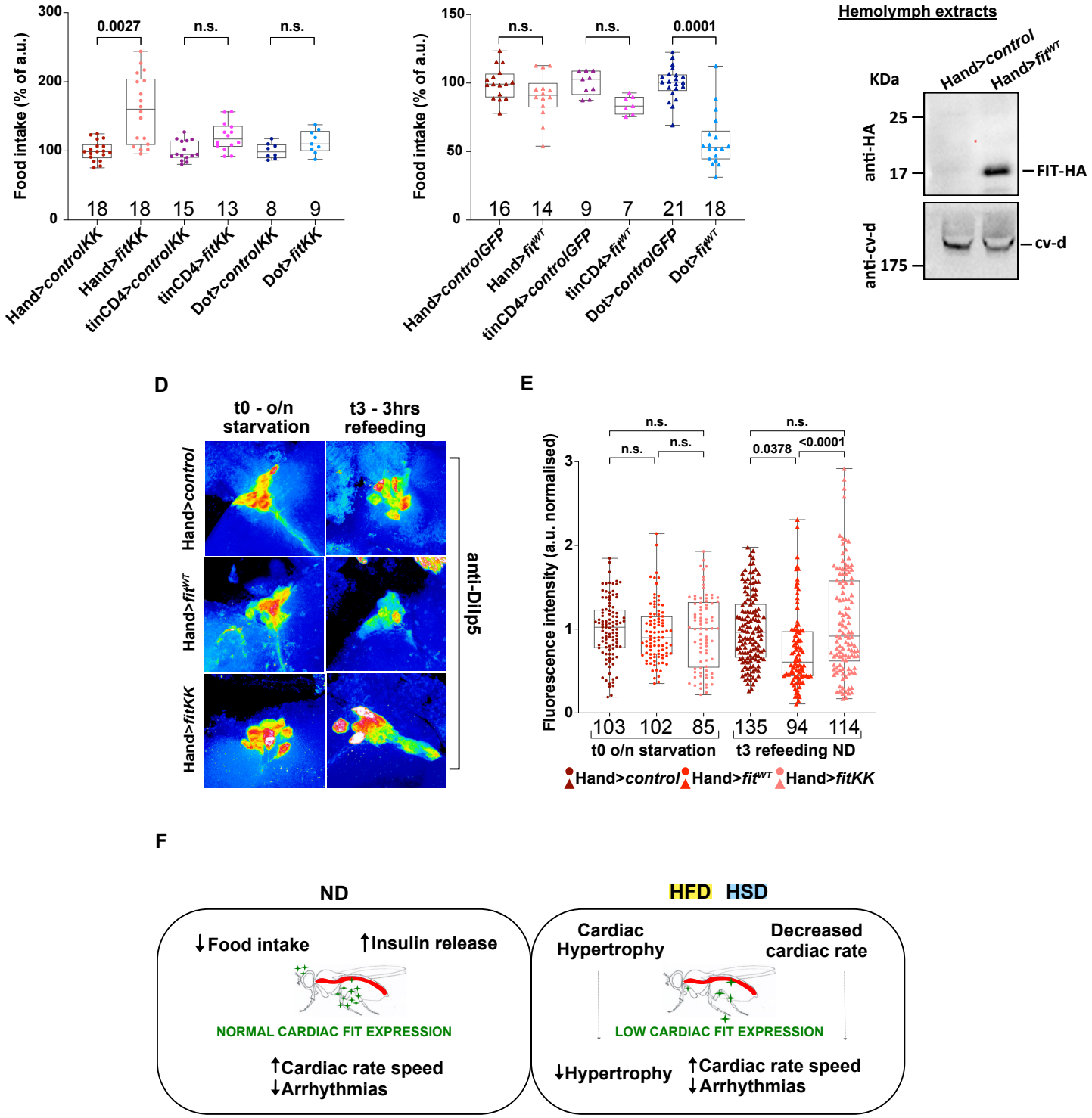

Figure 6